Mechanistic basis for LQT1 caused by S3 mutations in the KCNQ1 subunit of I_{Ks}

Jodene Eldstrom,[1] Hongjian Xu,[1] Daniel Werry,[1] Congbao Kang,[3] Matthew E. Loewen,[1] Amanda Degenhardt,[1] Shubhayan Sanatani,[2] Glen F. Tibbits,[4] Charles Sanders,[3] and David Fedida[1]

[1]Department of Anesthesiology, Pharmacology and Therapeutics, and [2]Department of Pediatrics, Children and Women's Hospital, University of British Columbia, Vancouver, British Columbia V6T 1Z3, Canada
[3]Department of Biochemistry, Vanderbilt University, Nashville, TN 37235
[4]Department of Biomedical Physiology and Kinesiology, Simon Fraser University, Burnaby, British Columbia V5A 1S6, Canada

Long QT interval syndrome (LQTS) type 1 (LQT1) has been reported to arise from mutations in the S3 domain of *KCNQ1*, but none of the seven S3 mutations in the literature have been characterized with respect to trafficking or biophysical deficiencies. Surface channel expression was studied using a proteinase K assay for *KCNQ1* D202H/N, I204F/M, V205M, S209F, and V215M coexpressed with *KCNE1* in mammalian cells. In each case, the majority of synthesized channel was found at the surface, but mutant I_{Ks} current density at +100 mV was reduced significantly for S209F, which showed ∼75% reduction over wild type (WT). All mutants except S209F showed positively shifted $V_{1/2}$'s of activation and slowed channel activation compared with WT ($V_{1/2}$ = +17.7 ± 2.4 mV and $\tau_{activation}$ of 729 ms at +20 mV; n = 18). Deactivation was also accelerated in all mutants versus WT (126 ± 8 ms at −50 mV; n = 27), and these changes led to marked loss of repolarizing currents during action potential clamps at 2 and 4 Hz, except again S209F. *KCNQ1* models localize these naturally occurring S3 mutants to the surface of the helices facing the other voltage sensor transmembrane domains and highlight inter-residue interactions involved in activation gating. V207M, currently classified as a polymorphism and facing lipid in the model, was indistinguishable from WT I_{Ks}. We conclude that S3 mutants of *KCNQ1* cause LQTS predominantly through biophysical effects on the gating of I_{Ks}, but some mutants also show protein stability/trafficking defects, which explains why the kinetic gain-of-function mutation S209F causes LQT1.

INTRODUCTION

Long QT interval syndrome (LQTS) is a potentially fatal condition, characterized by a prolonged QT interval (usually defined as longer than 440 ms for males and 460 ms for females on the electrocardiogram; Rossenbacker and Priori, 2007) and the development of serious arrhythmias (ventricular tachycardias and torsade de pointes, which may degenerate into ventricular fibrillation). Hereditary LQTS is predominantly caused by mutations in at least 12 (Lehnart et al., 2007; Tester and Ackerman, 2009) known genes that code for directly or are involved in the function of ion channels in the heart. Recent genome-wide association studies suggest that additional genes with small effects on the QT interval may contribute to the significant phenotypic variation seen in this syndrome (Arking et al., 2006; Newton-Cheh et al., 2009). Of the 12 ion channel or related genes, mutations in *KCNQ1* (LQT1), *hERG* (LQT2), and *SCN5A* (LQT3) are the most common, comprising ∼98% of all LQTS cases (Napolitano et al., 2005).

We have recently identified a novel missense mutation, V205M, in the S3 transmembrane region of *KCNQ1*, the α subunit for the slow delayed rectifier potassium channel, I_{Ks} (Sanguinetti et al., 1996). This mutation is present with a high prevalence, perhaps as high as 1:200, in an isolated Northern Canadian population that suffers a high incidence of sudden arrhythmic death (Arbour et al., 2008). V205M is not the only mutation associated with LQT1 found in the S3 domain of *KCNQ1* (Inherited Arrythmias Database [IAD]: http://www.fsm.it/cardmoc/), which also includes D202H/N, I204F/M, S209F, and V215M (Yamaguchi et al., 2003; Napolitano et al., 2005; Tester et al., 2005), but to our knowledge, none of these have been functionally characterized. Here, we studied all reported S3 mutations in *KCNQ1* in the presence of *KCNE1* electrophysiologically to better understand their role in the generation of LQTS in affected individuals. In addition, we sought to resolve the issue of whether V207M, also in the S3 domain, should remain as a polymorphism or be

Correspondence to David Fedida: fedida@interchange.ubc.ca

Abbreviations used in this paper: AP, action potential; IAD, inherited arrythmias database; LQTS, long QT interval syndrome; TMD, transmembrane domain; WT, wild-type.

© 2010 Eldstrom et al. This article is distributed under the terms of an Attribution–Noncommercial–Share Alike–No Mirror Sites license for the first six months after the publication date (see http://www.rupress.org/terms). After six months it is available under a Creative Commons License (Attribution–Noncommercial–Share Alike 3.0 Unported license, as described at http://creativecommons.org/licenses/by-nc-sa/3.0/).

The Rockefeller University Press $30.00
J. Gen. Physiol. Vol. 135 No. 5 433–448
www.jgp.org/cgi/doi/10.1085/jgp.200910351

The Journal of General Physiology

Downloaded from http://rupress.org/jgp/article-pdf/135/5/433/1788272/jgp_200910351.pdf by guest on 09 February 2026

reclassified as pathogenic. Originally, this mutation was found in one individual as part of a screen of 744 apparently healthy subjects (Ackerman et al., 2003). Subsequently, the same mutation was found in an individual during a screen of sudden unexplained death (Nishio et al., 2009). In mice homozygous for this mutation, the QT interval was significantly longer than in the wild-type (WT) mice, but no mention was made of whether arrhythmias or sudden unexplained death were observed in these animals. In the present study, we distinguished between mutations giving rise to LQTS primarily due to deficiencies in surface expression from those where LQTS was most likely to be caused by effects on KCNQ1 channel gating and kinetics and functional I_{Ks} currents.

The role and movement of the S3 helices within the voltage sensor are generally considered along with those of S4. From the recent crystal structure of Kv1.2 (Long et al., 2005), it is predicted that during activation, the voltage-sensing domain undergoes conformational changes with translation and rotation of S4 coupled with movement of the S1 to S3 helices around S4 (Yarov-Yarovoy et al., 2006). This is thought to allow for sequential interactions between basic residues in S4 and acidic residues in the S2 and S3 helices, which stabilize the charged residues in the hydrophobic environment of the membrane (Papazian et al., 1995; Tiwari-Woodruff et al., 2000). In addition to allowing for more sophisticated predictions for Kv channel activation, these crystal structures of Kv1.2 have enabled the generation of open- and closed-state models of KCNQ1, onto which many disease-causing mutations have been mapped (Smith et al., 2007) and KCNE1 interaction modeled (Kang et al., 2008). After we completed our electrophysiological analysis, the KCNQ1 models were used to examine the structural context of the residues in S3 that lead to LQTS and the other amino acid substitutions that we made at those sites. Modeling studies have informed the role of residue size, hydrophobicity, and charge on gating effects of S3 structures, as well as inter-residue van der Waals interactions and potential hydrogen bond formation. We suggest that such interactions between residues in S3 with those in S2 and S4 have significant effects on both closed- and open-state stability of the KCNQ1 channels and the resultant I_{Ks} currents, and that these changes have an important role in the causation of LQTS in affected individuals.

MATERIALS AND METHODS

Molecular biology

KCNQ1 and *KCNE1* genes were purchased from OriGene Technologies, Inc. Mutations within the third transmembrane (S3) region of the *KCNQ1* gene were constructed using two-step PCR reactions and sequenced to verify the presence of only the desired mutation.

Cell preparation and transfection

Electrophysiology was performed on transiently transfected mouse *ltk−* cells grown in MEM with 10% fetal bovine serum at 37°C in an air/5% CO_2 incubator. 1 d before transfection, cells were plated onto sterile glass coverslips in 35-mm Petri dishes with 20–30% confluence. On the day of transfection, cells were washed once with MEM with 10% fetal bovine serum. To identify the transfected cells efficiently, channel DNA was cotransfected with a vector encoding green fluorescent protein using the following DNA ratios: 1:2.5:1 in µg of *KCNQ1*/*KCNE1*/GFP and LipofectAMINE 2000 (Invitrogen). In some experiments, a mouse *ltk− KCNE1* stable line was used to express mutant and WT *KCNQ1* channels. Cells were allowed to grow overnight before recording.

Electrophysiological procedures

Coverslips containing cells were removed from the incubator before experiments and placed in a superfusion chamber (volume of 250 µl) containing the control bath solution at 35°C and perfused continuously with bathing solution heated to 35°C by an inline heater (Warner Instruments). Whole cell current recording and data analysis were done using an Axopatch 200B clamp amplifier and pClamp 8 and 10 software (MDS Analytical Technologies). Patch electrodes were fabricated using thin-walled borosilicate glass (World Precision Instruments, Inc.). Electrodes had resistances of 1–2 MΩ when filled with control filling solution. Capacity compensation and 80% series resistance compensation were used in all whole cell recordings. No leak subtraction was used when recording currents, and 0 current levels are denoted by the dashed lines in the current panels. Data were sampled at 10 kHz and filtered at 2 kHz. Membrane potentials have not been corrected for small liquid junction potentials between bath and pipette solutions. Action potential (AP) protocol was generated using LabHEART version 4.9.5.

TABLE I

LQT-associated mutants in the IAD

Nucleotide	Amino acid	Mutation type	Region	Phenotype	Reference
G604C	D202H	Missense	S3		Napolitano et al., 2005
G604A	D202N	Missense	S3	RWS	Yamaguchi et al., 2003
A610T	I204F	Missense	S3	RWS	Tester et al., 2005
C612G	I204M	Missense	S3		Napolitano et al., 2005
C626T	S209F	Missense	S3		Napolitano et al., 2005
G643A	V215M	Missense	S3		Napolitano et al., 2005

Amino acid numbering is based on Gene Bank cDNA:AF000571 and nucleotide numbering starts from ATG. RWS, Romano-Ward syndrome.

Downloaded from http://rupress.org/jgp/article-pdf/135/5/433/1788272/jgp_200910351.pdf by guest on 09 February 2026

Solutions

Patch pipettes contained (in mM): 130 KCl, 5 EGTA, 1 $MgCl_2$, 10 HEPES, 4 Na_2ATP, and 0.1 GTP, adjusted to pH 7.2 with KOH. The bath solution contained (in mM): 135 NaCl, 5 KCl, 10 HEPES, 2.8 sodium acetate, 1 $MgCl_2$, and 1 $CaCl_2$, adjusted to pH 7.4 with NaOH.

Data analysis

To determine the voltage dependence of activation, g-V plots were constructed using the normalized tail currents at −50 mV and fitted to a single Boltzmann function:

$$y = 1/(1 + \exp[(V_{1/2} - V)/k]),$$

where y is the conductance normalized with respect to the maximal conductance, $V_{1/2}$ is the half-activation potential, V is the test voltage, and k is the slope factor (RT/zF, where R is the gas constant, T is the absolute temperature, z is the valence, and F is the Faraday's constant). Single-exponential fits were used to obtain activation and deactivation time constants (see Table III and Fig. 5). It is recognized that activation is a complex process, but still we found empirically that >90% of the activation time course could be fit by a single-exponential process after allowing for the initial delay. Throughout the text, data are presented as mean ± SEM. Significance was tested using Student's unpaired t test or one-way ANOVA as appropriate.

To compare current densities at the respective $V_{1/2}$ for each mutant to that of WT (see Table II and Fig. 3 A), a correction factor was used to take into account the difference in driving force (DF) at each $V_{1/2}$. The current density (CD) at the $V_{1/2}$ for each mutant was corrected for driving force as follows. Corrected CD = CD at $V_{1/2} \times (DF_{WT}/DF_{Mt})$, where DF = $(V_{1/2} - E_{rev})$. The reversal potential (E_{rev}) used was −87.5 mV. An additional comparison of CD between mutants was made at +100 mV, where the P_o of channels is ≈1.0. These data are shown in Table II and are not corrected for DF.

Proteinase K and Western blot analysis

T7-tagged WT and mutant *KCNQ1* channels were expressed in a *KCNE1*-expressing mouse *ltk*− stable line. At 24 h, cells from half the flask were removed by scraping and the remainder were exposed to proteinase K as described previously (Manganas and Trimmer, 2000) to cleave any surface-expressed channel. Total protein was determined using a modified Lowry assay (Thermo Fisher Scientific), and equal amounts of total protein from proteinase K–untreated and -treated samples were loaded onto SDS-PAGE gels and probed with anti-KCNQ1 antibodies (Santa Cruz Biotechnology, Inc.).

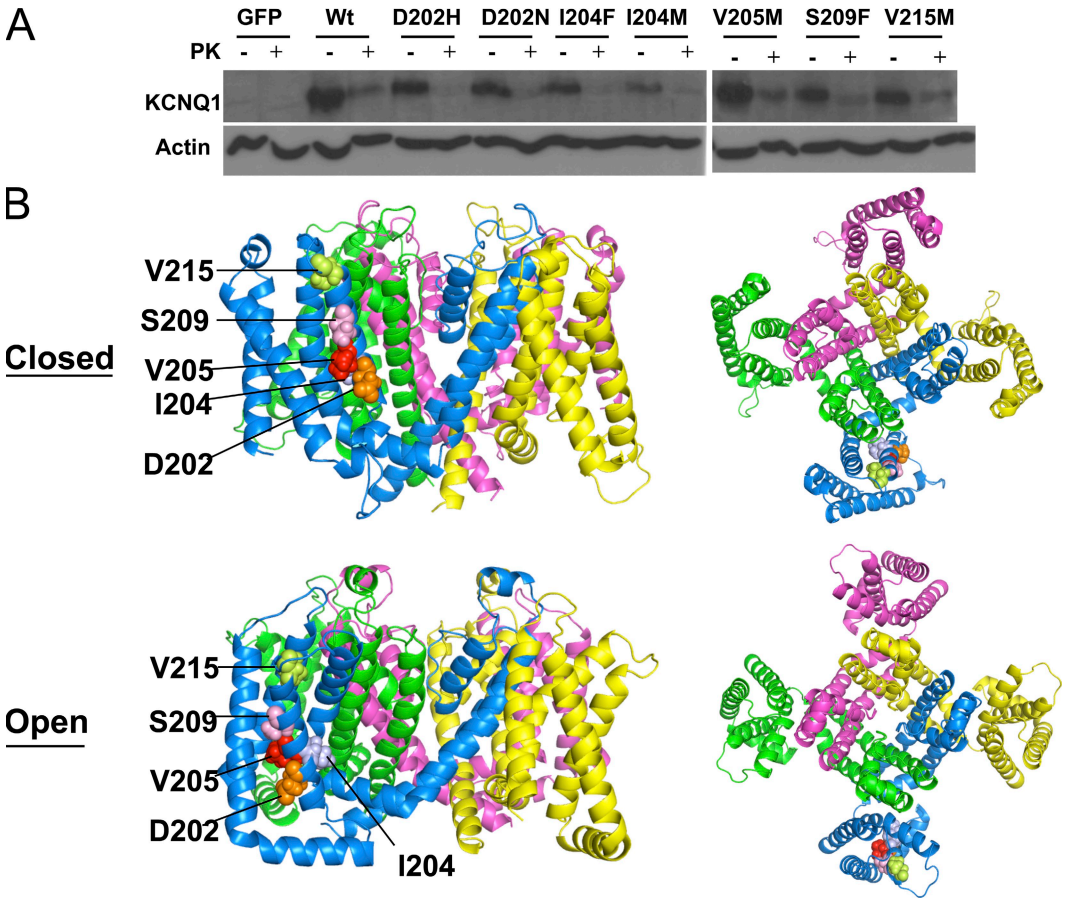

Figure 1. Reported LQT1-associated S3 mutants traffic to the plasma membrane in *ltk*− cells. (A) Western blot of WT and mutant *KCNQ1+KCNE1* proteins expressed in *ltk*− cells, untreated and treated with proteinase K (PK) to distinguish surface-expressed channel from internal. After normalization to actin for control of loading, the percent surface protein was determined from the density of bands before and after proteinase K treatment ($n = 3$) and was found to be: WT, 73%; D202H, 91%; D202N, 80%; I204F, 80%; I204M, 90%; V205M, 75%; S209F, 82%; V215M, 75%. (B) Model of *KCNQ1* tetrameric channels showing the locations of S3 mutations in space fill from the side and the extracellular face, with each subunit a different color.

Downloaded from http://rupress.org/jgp/article-pdf/135/5/433/1788272/jgp_200910351.pdf by guest on 09 February 2026

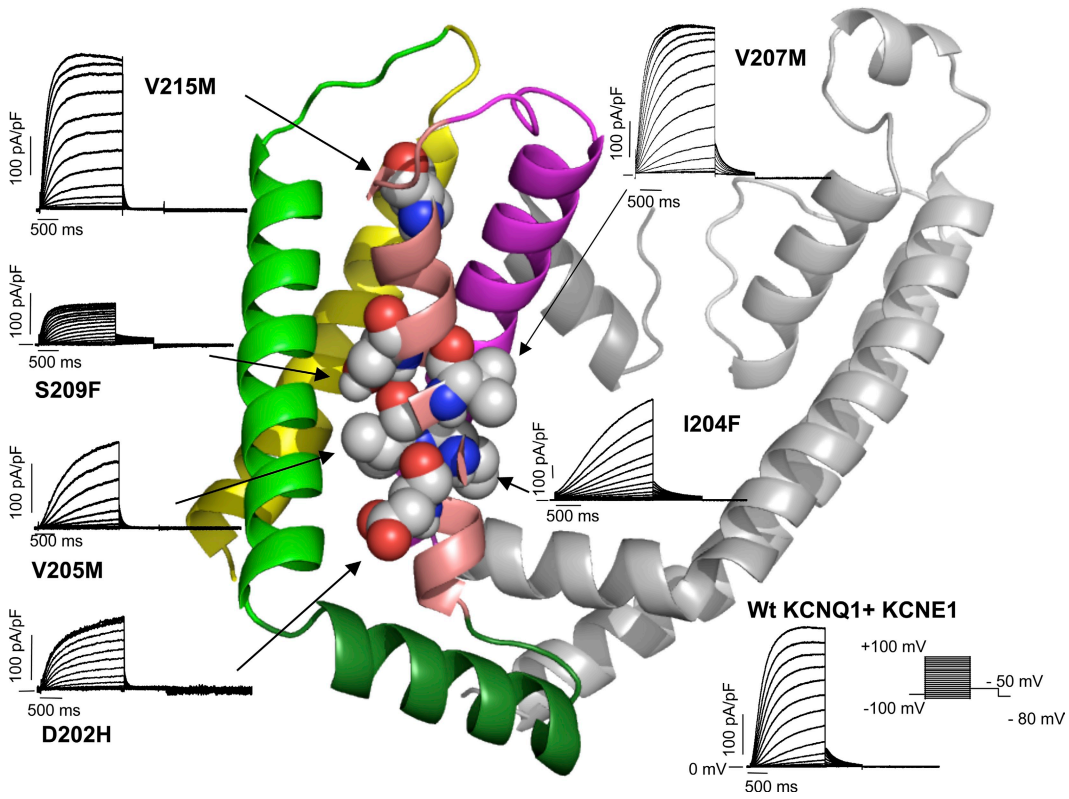

Figure 2. I_{Ks} current traces for WT and S3 KCNQ1 mutants. WT *KCNQ1+KCNE1* or mutant *KCNQ1+KCNE1* ionic currents were recorded at 35°C during 2-s depolarizing pulses to between −100 and +100 mV, followed by a 1-s repolarizing pulse to −50 mV. Cartoon is of KCNQ1 in the open state, with residues in which mutations have been identified in S3 represented in space fill. Only one subunit is shown, except for the filter and pore helix of an adjacent subunit for orientation purposes. The color scheme is as follows: yellow, S1; green, S2; salmon, S3; magenta, S4; the rest of the subunit is gray.

Molecular modeling of WT and mutant channels

As described previously (Smith et al., 2007), models for the open and closed states of the channel domain (S1–S6) of human KCNQ1 were developed using a combination of homology-based modeling (using available Kv1.2 structures as templates) and ROSETTA-based structure prediction (Das and Baker, 2008) to define segments that could not be well-defined based on the Kv1.2 structures. These models are available online from Smith et al. (2007).

Models for the mutant channels were developed using the WT models noted above as the starting point and using RosettaDesign (Kuhlman and Baker, 2000). The mutated channels were then subjected to five cycles of side chain repacking and gradient energy minimization, by which point the energy and coordinates of the structures converged. Mutants were typically analyzed using "contact analysis" in which inter-residue van der Waals interactions involving a designated (often mutated) site were assessed by determining which other residues in the protein have at least

TABLE II

$V_{1/2}$ and I_{Ks} current density at various potentials for WT and mutant KCNQ1 channels expressed with KCNE1

Variant	$V_{1/2}$	Current density (pA/pF)					
	mV	0 mV	20 mV	at $V_{1/2}$	*n*	100 mV	*n*
WT	17.7 ± 2.4	92.1 ± 15.4	215.3 ± 25.4	215.3 ± 25.4	47	488.3 ± 52.8	25
D202H	34.3 ± 5.3	35.4 ± 7.0	88.9 ± 16.0	104.3 ± 18.6[a]	24	311.7 ± 56.2	15
D202N	41.5 ± 2.9	9.4 ± 1.8	43.9 ± 9.3	98.6 ± 18.6[a]	20	326.6 ± 59.7	14
I204F	71.0 ± 3.9	24.2 ± 11.4	49.8 ± 17.1	172.6 ± 32.8	22	424.1 ± 64.2	12
I204M	53.8 ± 2.6	21.2 ± 7.2	72.8 ± 16.3	157.9 ± 26.2	21	337.3 ± 46.1	16
V205M	37.0 ± 5.4	26.8 ± 4.4	78.4 ± 11.5	134.7 ± 17.8[a]	38	344.6 ± 56.5	21
S209F	−31.0 ± 2.3	59.1 ± 9.1	75.7 ± 11.4	54.1 ± 8.3[a]	25	121.4 ± 17.8[a]	17
V215M	37.9 ± 4.3	18.8 ± 3.9	82.7 ± 20.0	172.0 ± 41.5	22	450.1 ± 84.8	17
V207M	24.8 ± 2.9	85.7 ± 17.6	200.1 ± 32.3	200.1 ± 32.3	20	486.9 ± 51.7	17

Current densities at $V_{1/2}$ for each mutant channel were corrected for difference in driving force from WT (see Materials and methods). Only current densities at $V_{1/2}$ and 100 mV were tested for significance.
[a]$P < 0.05$ compared to WT.

Downloaded from http://rupress.org/jgp/article-pdf/135/5/433/1788272/jgp_200910351.pdf by guest on 09 February 2026

one atom within 4 Å of at least one atom of the designated site. A home-written script for use with PyMOL was created for this purpose. Structures were also visualized using PyMOL (DeLano, 2002).

Online supplemental material

The online supplemental material includes a table of current densities of I_{Ks} for all D202 mutants made (Table S1), detailed kinetics of S3 domain mutation V207M (Fig. S1), and V207M I_{Ks} activity during a simulated cardiac AP (Fig. S2) compared with WT. In addition, we show the results of contact analysis for residues of interest (R195, D202, and 205) in S2 and S3 and the S2–S3 linker from the KCNQ1 homology model for WT, V205L/M/A (Table S2). In Fig. S3, we show a close-up of the molecular interactions for V205 from the model in the open and closed states. The supplemental material is available at http://www.jgp.org/cgi/content/full/jgp.200910351/DC1.

RESULTS

LQTS due to trafficking versus biophysical defects

The IAD lists several mutations in the S3 domain (which comprises approximately amino acids Ile 198 to Val 215) of KCNQ1 that have been linked to LQTS (Table I). These mutations span the entire length of the S3 domain (Figs. 1 B and 2), with six of the seven (including V205M; Arbour et al., 2008) predicted to line one face of the S3 helix in an open-state homology model of KCNQ1 (Smith et al., 2007). In addition, the IAD lists one S3 polymorphism, V207M, which in our models is predicted to face lipid (Fig. 2). We were interested in studying this mutant not only as it represented an opportunity to test the KCNQ1 model, but also, as noted previously, the literature was inconsistent as to the proper classification, polymorphism or pathogenic (Ackerman et al., 2003; Nishio et al., 2009).

Initially, we wanted to explore the possibility that these mutations lead to trafficking defective protein, so T7-tagged WT and mutant KCNQ1 channels were expressed in a KCNE1 (E1)-expressing mouse *ltk*− stable line. At 24 h, cells from half the flask were removed by scraping and the remainder exposed to proteinase K to cleave any surface-expressed channel. Western blots of untreated and proteinase K–treated samples show that WT and all mutant channels, D202H/N, I204F/M, V205M, S209F, and V215M, express significantly at the surface, as the majority of the 70-Kd KCNQ1 band is cleaved by proteinase K (Fig. 1 A). Densitometric analysis revealed that, normalized to actin, 10–25% of mutant protein was not digested by proteinase K, compared with 27% of WT protein ($n = 3$ and P = NS), suggesting that the S3 mutations do not significantly affect channel trafficking per se. Although the cell surface ratio of the S209F mutant was similar to WT, this mutant consistently showed lower levels of total protein, suggesting that perhaps protein stability was an issue for this mutant. The Western blot data were generally supported by current density measurements from patch clamp experiments (Table II). Current densities were calculated at four potentials: at the $V_{1/2}$ of activation, as measured from 2-s activation relationships after correction for driving force (see Materials and methods and Fig. 3 A), and at 0 and +20 mV, which are two potentials relevant to the plateau of the cardiac AP, where changes in current density and gating are likely to have the most significant effects on repolarization. In addition, current

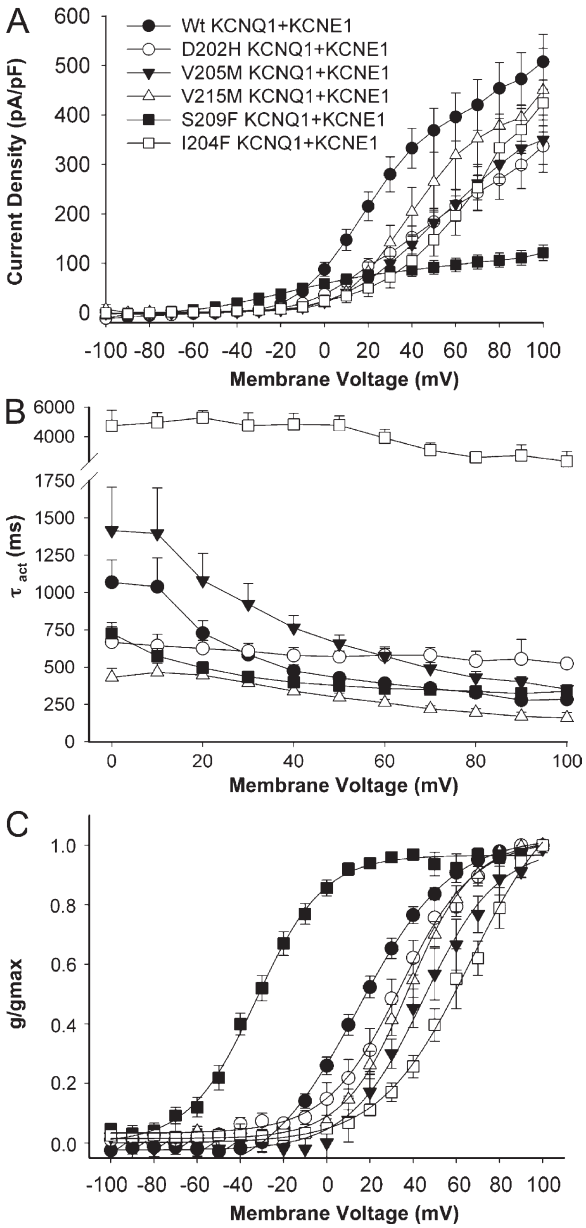

Figure 3. I_{Ks} current density and detailed activation kinetics of S3 domain KCNQ1 mutants. (A) Current densities for WT and mutant *KCNQ1+KCNE1*-transfected cells at each potential. (B) Activation time constants (τ_{act}) from fits to currents in Fig. 2 at each potential (WT, $n = 17$; D202H, $n = 7$; V205M, $n = 7$; I204F, $n = 8$; S209F, $n = 8$; V215M, $n = 7$–11). (C) g-V relationships from the peak tail currents. In all cases, measurements were made from currents recorded using the protocols described in the legend to Fig. 2.

Downloaded from http://rupress.org/jgp/article-pdf/135/5/433/1788272/jgp_200910351.pdf by guest on 09 February 2026

densities were measured at 100 mV, where activation curves were saturated or near to saturated, and in this situation, only S209F showed a significantly reduced current density compared with WT. At their $V_{1/2}$'s of activation (Table II), D202H/N and V205M-expressing cells had ~46–60% less current and S209F-expressing cells had ~25% of the WT current level, but other mutants tested had normal currents, which suggested that biophysical factors might be responsible for the LQTS observed in individuals affected by these mutations, and prompted the further studies described below. In all the mutants, with the exception of V207M, it appears that the combination of reduced overall expression and positively shifted $V_{1/2}$'s of activation causes the reduction in absolute measured currents at 0 and +20 mV.

S3 mutations alter activation and deactivation properties of I_{Ks} channels

The response of WT and mutant I_{Ks} to voltage was tested by expression at 35°C in mouse *ltk*− cells, as these cells have no detectable endogenous potassium current. WT I_{Ks} activated slowly upon depolarization from a holding potential of −100 mV and showed little inactivation over a 2-s pulse (Fig. 2). I_{Ks} made up from D202H mutants showed smaller currents with a similar activation time course to WT over the physiological range of voltages. Interestingly, the activation time constants did not decrease significantly at more positive potentials, unlike WT (Fig. 3 B), and this was accompanied by a positive shift in the $V_{1/2}$ of activation of 17 mV from WT (Fig. 3 C). The combination of the positive displacement of the activation relationship and the lower overall expression (Fig. 3 and Table II) resulted in much reduced peak currents in D202H in the physiological range of plateau potentials, 0 and +20 mV (Table II and Fig. 3 A).

In addition to modulating I_{Ks} channel activation properties, the D202H mutation accelerated the rate of channel deactivation compared with WT (Fig. 4). The time constant of deactivation was determined by applying hyperpolarizing steps after a prepulse to +80 mV and fitting the tail currents between −40 and −100 mV to single-exponential functions (Fig. 4 B). It is clear that the D202H mutation accelerated deactivation at all the potentials tested compared with WT channels. These data suggest that the D202H mutation reduces I_{Ks} channel availability by shifting the voltage dependence of activation to more depolarized potentials, in addition to moderately slowing activation at positive potentials and accelerating the rate of channel deactivation.

The electrophysiological data from a scan of other mutations at D202 are shown in Table III, along with residue properties such as volume, hydrophobicity, and charge. Charge reversal, as in D202H or D202K, resulted in channels that did not express as well as WT (Table S1) and suffered similar depolarizing shifts in

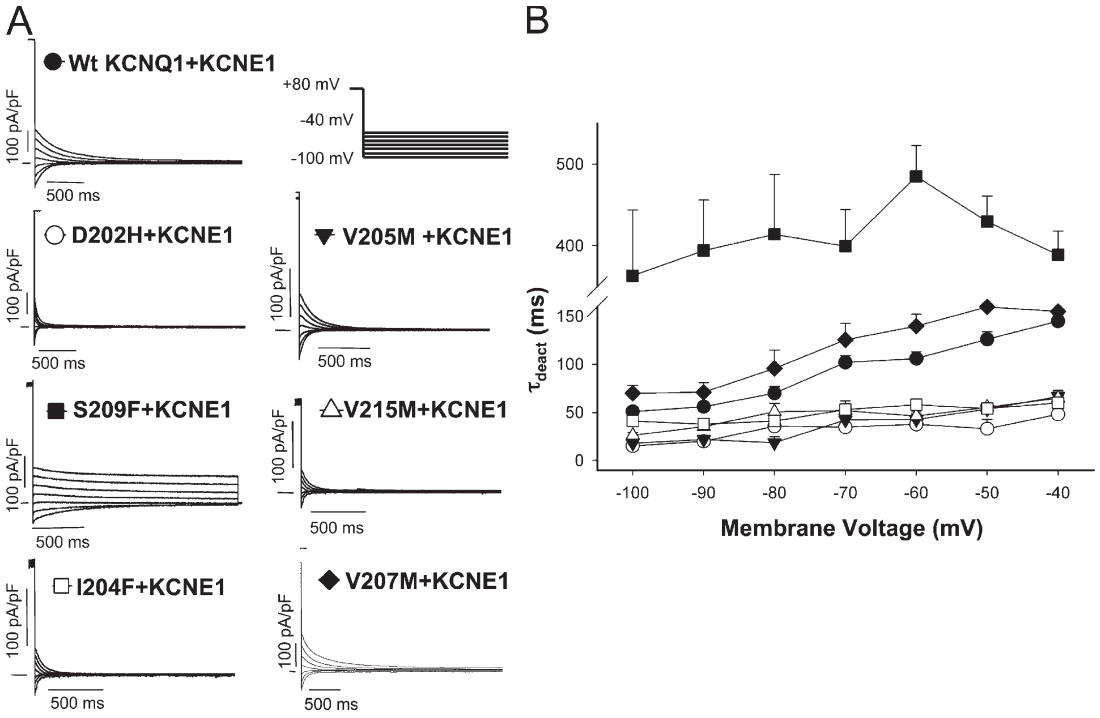

Figure 4. I_{Ks} deactivation tail currents and time constants of S3 KCNQ1 mutants. (A) Deactivation of WT or mutant KCNQ1+KCNE1 ionic currents was recorded at 35°C during repolarization to potentials between −40 and −100 mV in 10-mV increments after 3-s depolarizing pulses to +80 mV. (B) Time constants (τ_{deact}) were from single-exponential fits to tail currents and are plotted versus membrane potential (WT, $n = 25$; D202H, $n = 5$; V205M, $n = 7$; I204F, $n = 8$; S209F, $n = 10$; V215M, $n = 7$–11).

Downloaded from http://rupress.org/jgp/article-pdf/135/5/433/1788272/jgp_200910351.pdf by guest on 09 February 2026

the $V_{1/2}$ of activation to about +40 mV, without much change in the activation time constants at either +20 mV or at the $V_{1/2}$ activation, and a clearly accelerated deactivation. It is less obvious why the D202E charge-conserving mutation results in such an extreme shift in the $V_{1/2}$ activation (to +72 mV) and accelerated deactivation. The other naturally occurring mutant at this position in S3 results in neutralization of the charge, D202N. This mutation results in a channel that could express almost as well as WT (Table II) and has the effect of accelerating activation and showing extremely rapid deactivation kinetics (Table III). These data suggest that stability of both the open and the closed states may have been affected by the loss of charge (see below). In addition, in this mutant as was seen with D202H (Figs. 3 B and 4 B), both activation and deactivation curves have relatively little apparent voltage dependence (not depicted).

Representative data and summary tables for the electrophysiological properties of the other naturally occurring LQTS mutants, V205M, S209F, V215M, V207M, and I204F/M, are also shown in Figs. 2–4, Table III, and Fig. S1, as well as properties of other substitutions made at these sites. The mean changes in the activation and deactivation time constants relative to control are shown in Fig. 5. It can be seen that naturally occurring mutations, as well as those introduced during the study into the middle of the helix, at V205 and I204 cause the most slowing of channel activation, whereas the mutations toward the proximal and distal ends of S3, at D202 and V215, either have little effect on activation or speed it somewhat. In contrast, all the mutations, with the exception of those at S209, I204A, and V215A, accelerate deactivation, often substantially as seen at D202, V205, and V215. Little kinetic effect of the V207M mutation is apparent. All of the naturally occurring mutations except V207M and S209F caused a positive shift of the $V_{1/2}$ activation from WT, with values ranging from +37 and +38 mV in V205M and V215M, respectively, like the D202 mutants, to more extreme values of +54 and +71 mV in the I204M and I204F mutants, respectively (Fig. 5). At I204, mutations and substitutions (I204A/N)

TABLE III

Summary data for various mutants including amino acid properties, as stated for each mutation

Variant	Volume	Hydrophobicity		τ_{act}		τ_{deact}	$V_{1/2}$ of activation	Slope
	Å^3		Charge	20 mV	at $V_{1/2}$	−50 mV		
				ms	*ms*	*ms*	*mV*	
D202	111.1	−3.5	Negative	729	729	126	17.7 ± 2.4	17.2 ± 1.0
D202N	114.1	−3.5	Neutral	400	392	11	41.5 ± 2.9[a]	14.0 ± 1.5
D202H	153.2	−3.2	Pos/Neu	607	600	33	34.3 ± 5.3[b]	14.5 ± 2.0
D202A	88.6	1.8	Neutral	644	604	44	29.8 ± 2.9	20.0 ± 2.2
D202E	138.4	−3.5	Negative	728	739	42	72.3 ± 3.4[a]	17.2 ± 1.9
D202M	162.9	1.9	Neutral	738	799	28	41.2 ± 2.9[a]	14.6 ± 1.5
D202K	168.6	−3.9	Positive	878	878	61	39.5 ± 3.9[a]	11.5 ± 1.4[b]
I204	166.7	3.8		729	729	126	17.7 ± 2.4	17.2 ± 1.0
I204M	162.9	1.9		845	768	82	53.8 ± 2.6[a]	16.2 ± 0.6
I204F	189.9	2.8		5,287[c]	3,083[c]	54	71.0 ± 3.9[a]	18.5 ± 2.0
I204A	88.6	1.8		1,511	925	170	36.4 ± 3.3[a]	12.0 ± 1.1
I204N	114.1	−3.5		1,802	1,375	88	50.6 ± 9.8[a]	16.0 ± 1.9
V205	140	4.2		729	729	126	17.7 ± 2.4	17.2 ± 1.0
V205M	162.9	1.9		1,081	825	53	37.0 ± 5.4[a]	17.3 ± 2.2
V205L	166.7	3.8		333	507	75	0 ± 3.3	9.7 ± 0.6[a]
V205A	88.6	1.8		915	1,332	52	68.8 ± 7.7[a]	12.3 ± 2.0
S209	89	−0.8		729	729	126	17.7 ± 2.4	17.2 ± 1.0
S209F	189.9	2.8		496	1,902	430	−31.0 ± 2.3[a]	14.9 ± 1.2
S209M	162.9	1.9		617	1,666	420	−22.6 ± 3.7[a]	15.0 ± 0.9
S209A	88.6	1.8		295	650	302	−16.3 ± 3.9[a]	15.0 ± 1.2
S209L	166.7	3.8		803	2,357	352	−30.1 ± 4.7[a]	15.7 ± 2.3
V215	140	4.2		729	729	126	17.7 ± 2.4	17.2 ± 1.0
V215M	162.9	1.9		448	340	55	37.9 ± 4.3[b]	14.4 ± 0.6
V215A	88.6	1.8		501	564	331	8.4 ± 2.3	14.0 ± 1.0
V215L	166.7	3.8		459	411	85	27.9 ± 4.3	13.6 ± 1.5
V215P	112.7	−1.6		593	551	29	55.7 ± 4.4[a]	12.2 ± 0.9

Hydrophobicity was based on the Kyte Doolittle scale, and other values were obtained as indicated in the legend to Fig. 2.
[a]Significant difference from WT ($P < 0.01$).
[b]Significant difference from WT ($P < 0.05$).
[c]τ_{act} for I204F activation was measured at 6 s rather than 2 s due to this process being very slow. Only $V_{1/2}$ values were tested for significance.

Downloaded from http://rupress.org/jgp/article-pdf/135/5/433/1788272/jgp_200910351.pdf by guest on 09 February 2026

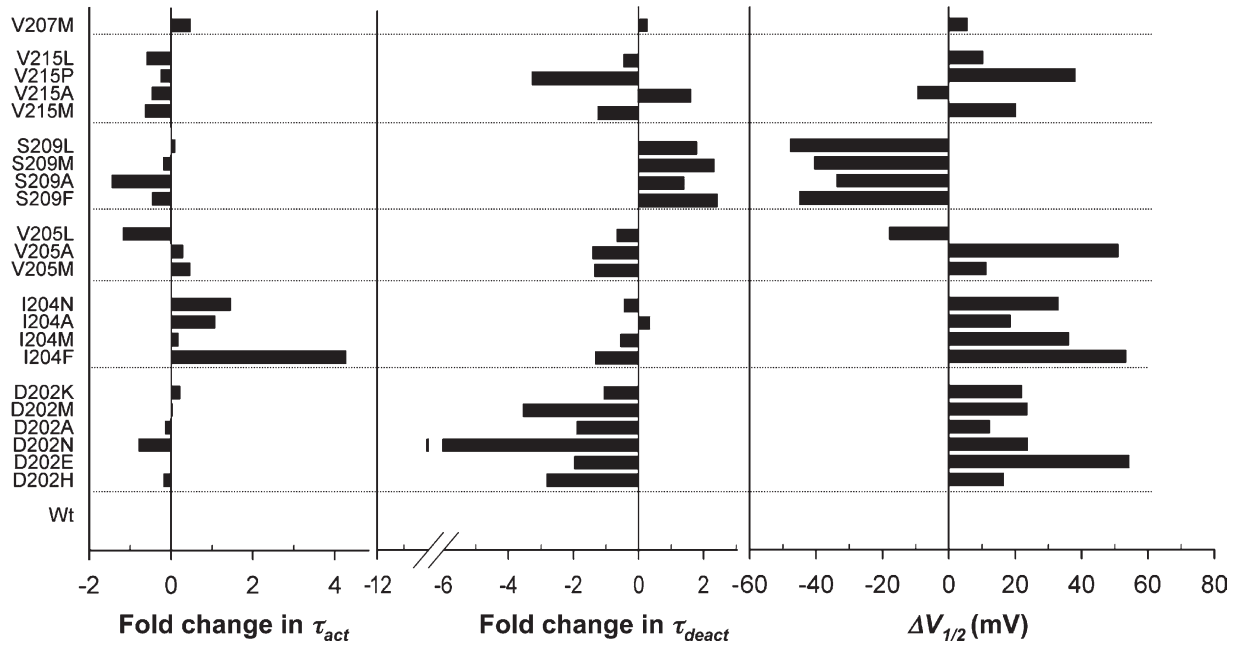

Figure 5. Fold changes in activation and deactivation time constants and the $V_{1/2}$ of activation for I_{Ks} resulting from mutations in S3. Fold change from WT for activation time constants at +20 mV and deactivation time constants at −50 mV for all S3 mutants. See Materials and methods for calculation of time constants. Change in the $V_{1/2}$ of activation from WT for each of the S3 mutants is shown.

uniformly displaced activation to more positive potentials, greatly slowed activation kinetics, particularly for I204F (Figs. 2 and 3 B) and only moderately in I204M (Table III and Fig. 5), and, with the exception of I204A, accelerated deactivation moderately (Fig. 5). At position V205, less hydrophobic substitutions V205M and V205A shifted activation to more positive potentials, moderately slowed activation time constants, and accelerated deactivation (Figs. 2–5). The bulky and hydrophobic substitution, V205L, shifted activation to more negative potentials even than WT and accelerated both activation and deactivation (Table III and Fig. 5), essentially reversing the effect of V205M. At V215, the naturally occurring mutation V215M did shift activation to a $V_{1/2}$ of +37 mV, but surprisingly, it accelerated both activation and deactivation time constants over WT (Figs. 3 B, 4 B, and 5). In fact, all substitutions tested at V215, except V215A, positively displaced the activation curve compared with WT and similarly accelerated activation and deactivation time constants over control. V215A, which is a low volume substitution, also accelerated activation like the other mutants at this position, but it shifted the $V_{1/2}$ activation to more negative potentials (+8.4 mV) than WT and slowed deactivation threefold at −50 mV, which is essentially the opposite action to V215M (Table III). Consistent with a position on the side of the S3 helix facing away from the rest of the voltage sensor transmembrane domains (TMDs), the V207M polymorphism is essentially equivalent to WT in both functional expression and kinetic properties (Table II and Figs. S1 and S2).

S209F is a gain-of-function mutant

Of the naturally occurring mutants in S3, S209F is a much bulkier and more hydrophobic residue than the WT serine, and it produced dramatic changes in channel kinetics (Figs. 3 and 4). Overall, current expression was reduced in this mutant (Fig. 3 A and Table II), but most interesting was the marked hyperpolarizing shift of channel activation ($V_{1/2}$ = −31.0 mV; Figs. 3 C and 5). As a result of this shift, the activation time constants were accelerated at physiological potentials, but overall, opening was slowed as suggested by the greatly delayed activation time course at the $V_{1/2}$ activation (time constant was 1.9 s vs. 730 ms in WT). The deactivation was extremely slow for S209F, at ∼400 ms, and was quite voltage independent (see Fig. 4 B). Similar kinetic properties were seen in the other substitutions at S209, with all showing $V_{1/2}$'s of activation in the negative range of potentials (Fig. 5) and very slow deactivation (Fig. 5 and Table III). Only S209A showed more normal activation kinetics, with activation time constants close to WT at the $V_{1/2}$, and it had a $V_{1/2}$ activation closer to the WT than other bulkier substitutions (Table III). Activation time constants were much faster when S209F was expressed alone (87.6 ± 5.0 ms at +20 mV compared with 496 ms for S209F+E1; Fig. 6), despite the fact that the voltage dependence of activation was relatively unaffected by coexpression of S209F with KCNE1 (Fig. 6 C). The clear slowing of the activation time course (Fig. 6 A) and the slowed time constants indicate that the negative shift in activation was not a result of failure to coassemble with KCNE1.

Downloaded from http://rupress.org/jgp/article-pdf/135/5/433/1788272/jgp_200910351.pdf by guest on 09 February 2026

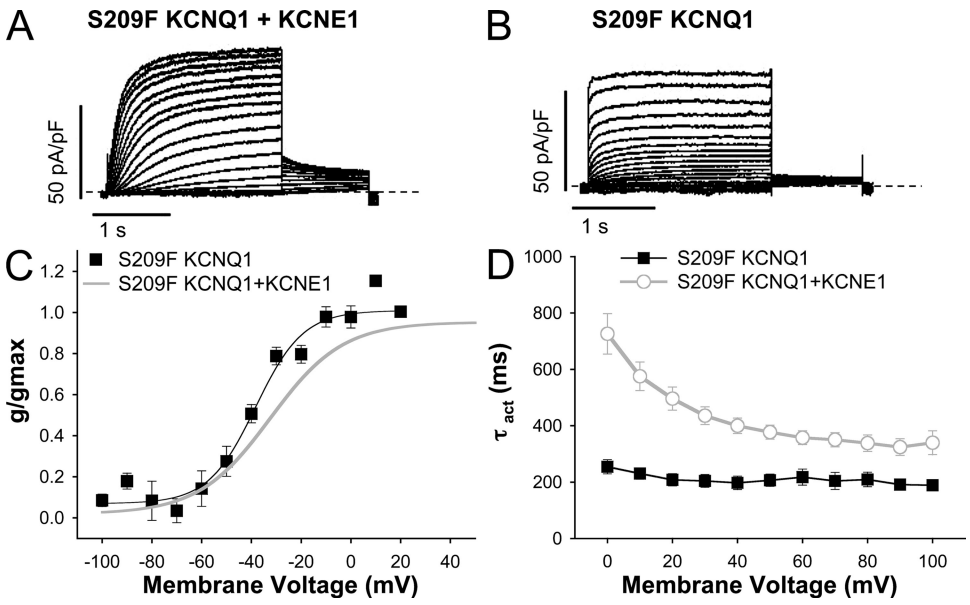

Figure 6. Comparison of S209F currents with and without KCNE1. (A) S209F+*KCNE1* or (B) S209F without KCNE1 ionic currents were recorded at 35°C during 2-s depolarizing pulses to between −100 and +100 mV, followed by a 1-s repolarizing pulse to −50 mV. (C) g-V relationships from the peak tail currents. The $V_{1/2}$ of activation and slope factor was −39.0 ± 4.3 and 16.6 ± 2.3 for S209F and −31.0 ± 2.3 and 14.9 ± 1.2 for S209F+KCNE1. (D) Activation time constants (τ_{act}) from fits to currents (A and B) at each potential (S209F+KCNE1, $n = 8$; S209F alone, $n = 5$). Note that for S209F expressed alone, the cells were cultured at 30°C to rescue expression; coexpressing with KCNE1 allowed expression at a culture temperature of 37°C.

S3 mutant channels during simulated cardiac APs

Overall, these findings suggested that charge and volume were important regulators of activation and deactivation gating at D202 and hydrophobicity at V205 in the S3 of KCNQ1, but that size and/or polar/hydrophobicity were important regulators of gating at residues higher up S3, like S209 and V215. To better understand the contribution of I_{Ks} with the S3 mutants to repolarization, currents were recorded from WT I_{Ks} and the naturally occurring mutant I_{Ks} channels D202N and S209F *KCNQ1+E1* during simulated ventricular APs (Figs. 7 and 8). The clamp protocol (Fig. 7 A) at 2 Hz produced

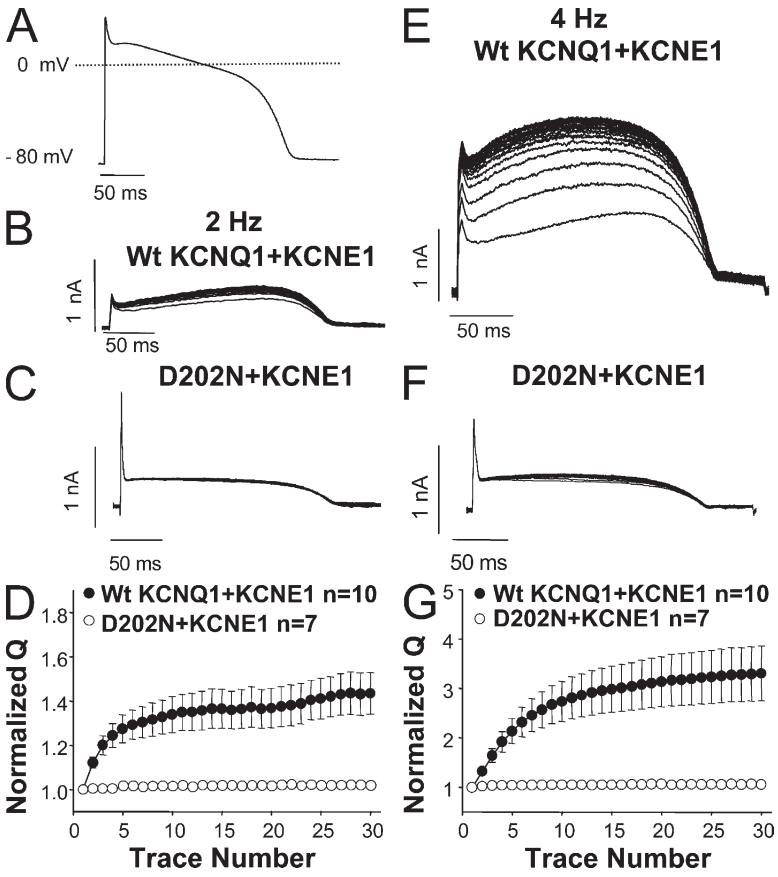

Figure 7. D202N eliminates I_{Ks} during a simulated cardiac AP. Typical currents recorded at 35°C from cells expressing WT (B) or D202N *KCNQ1+KCNE1* (C) channels during a ventricular AP clamp (duration of 230 ms; LabHeart version 4.9.5) (A) applied at 2 Hz. (D) Charge from integrated current waveforms during the AP protocol compared between WT and D202N I_{Ks}. Data were normalized to the total charge during the first AP. Currents recorded during 4-Hz ventricular AP clamp to WT (E) or D202N (F) cells. (G) Charge movement at 4 Hz was quantitated as in D. Total charge from D202N channels was significantly reduced compared with WT channels, at both 2 and 4 Hz ($P < 0.001$).

Downloaded from http://rupress.org/jgp/article-pdf/135/5/433/1788272/jgp_200910351.pdf by guest on 09 February 2026

a bell-shaped WT I_{Ks} waveform in channels with relatively slow activation kinetics and a peak of ionic current during the repolarization phase of the AP. During the second and subsequent APs, currents were potentiated (Fig. 7 B) and the total charge movement, estimated by integrating currents during the AP (Fig. 7 D), increased by ~40% during pulsing to a steady state, compared with the first. In sharp contrast, D202N channels displayed little detectable ionic current due to I_{ks} during the AP (Fig. 7 C), with most of the current comprising leak currents; thus, total charge during the simulated AP was effectively 0% of that for WT channels.

The shifted $V_{1/2}$ of activation, slowed activation, and the accelerated deactivation in the D202N mutant all reduced the number of open I_{Ks} channels during rapid AP firing. At 4 Hz, in the WT channels, the current amplitude at the beginning of the pulse was increased, as was the overall current envelope (Fig. 7 E), and the outward charge movement (+338 ± 7%; n = 12) increased from the first pulse (Fig. 7 G). In cells expressing D202N I_{Ks}, there were only small currents during APs (Fig. 7 F), and the outward charge did not increase at 4 Hz (Fig. 7 G; n = 7).

Similar results were found for the D202H, I204M/F, V205M, and V215M mutants (not depicted), as expected from their slowed activation and accelerated deactivation kinetics shown in prior figures. However, it was of interest to examine the effect of AP clamps on the S209F gain-of-function mutant (Fig. 8). Here, it is apparent that the rapid activation kinetics in the plateau range of potentials and the persistent activation can give rise to a significant potentiation of currents during 2-Hz stimulation (Fig. 8 C) compared with WT (Fig. 8 B). The rapid S209F kinetics also change the shape of currents during the AP so that it closely matches the waveform shape, rather than developing during the plateau and repolarization like the WT I_{Ks}. At 4 Hz, S209F I_{Ks} currents summate much like they do at 2 Hz and like WT channels, so that the normalized charge is much the same in WT and mutant channels at high stimulus rates (Fig. 8 G). Notably, the shortened interpulse interval at 4 Hz negates the more rapid deactivation in WT channels compared with S209F. Still, the more rapid activation of S209F channels gives a current waveform biased to more depolarized potentials early in phases 1 and 2 of the AP, rather than phase 3, where the dominant repolarization current appears in the WT channels.

The V207M polymorphism, which shows no significant kinetic difference from WT I_{Ks}, is indistinguishable from WT I_{Ks} during simulated AP clamps (Fig. S2).

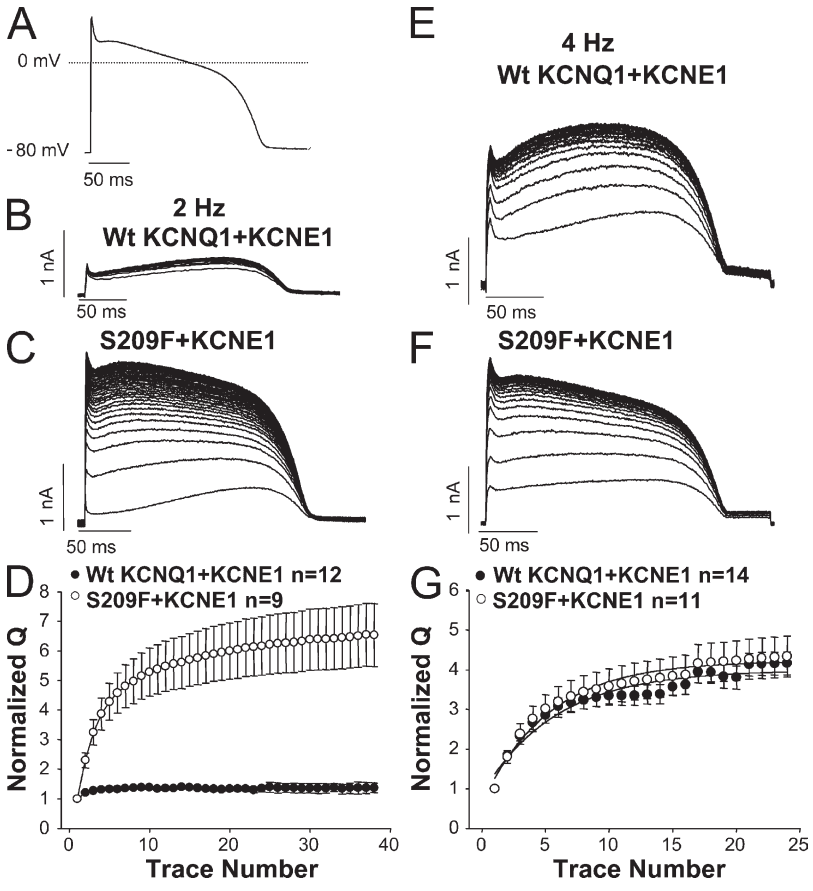

Figure 8. S209F increases I_{Ks} during simulated cardiac APs. Protocol as for Fig. 7. 2-Hz currents from cells expressing WT I_{Ks} (B) or S209F I_{Ks} (C) during simulated AP clamps (A). (D) Normalized charge during the AP protocol for WT and S209F I_{Ks} ($P < 0.001$). 4-Hz AP clamp currents in WT (E) or S209F (F) cells. (G) Charge movement at 4 Hz was not significantly different between WT and S209F ($P > 0.05$).

Downloaded from http://rupress.org/jgp/article-pdf/135/5/433/1788272/jgp_200910351.pdf by guest on 09 February 2026

DISCUSSION

S3 mutant subunits of I_{Ks} express well at the cell surface

The majority of *KCNQ1* mutations produce a loss of function by disrupting protein folding, assembly, and/or trafficking to the membrane (Shalaby et al., 1997; Dahimène et al., 2006). In our cell expression system, all the naturally occurring mutants expressed at the surface as determined by the proteinase K assay, with no significant changes in the surface/intracellular protein ratios. At +100 mV, only the S209F mutation showed a significantly decreased expressed current density over WT, although reduced current densities at the $V_{1/2}$ of activation were found electrophysiologically for D202H/N, V205M, and S209F (Table II). It may be that the very slowed activation in the V205M and D202H/N mutants (Figs. 2 and 3) leads to incomplete activation of currents at the most positive potentials, an underestimation of the $V_{1/2}$ of activation in these mutants, and an apparently reduced current density at the $V_{1/2}$. However, no mutation at the S3 sites, in addition to those reported in the IAD, resulted in channels with WT kinetic properties. This suggests that the major defects with the remaining LQTS-associated S3 mutants are kinetic, although we cannot rule out the possibility that trafficking efficiency is reduced in the native myocyte, perhaps with a larger proportion of channels undergoing ER-associated degradation due to increased folding times (Ellgaard and Helenius, 2003).

Altered kinetics of S3 mutants

The face of the KCNQ1 S3 helix lined by D202, V205, I204, S209, and V215 (Figs. 1 and 2) appears to be kinetically sensitive to mutation, which likely indicates extensive interaction with the other transmembrane domains of the voltage sensor. This was in contrast to the V207M mutant, predicted to face lipid in the model, which was identical to WT in its kinetic properties and current density (Fig. 5, Figs. S2 and S3, and Tables II and III), and consistent with its classification as a polymorphism in the IAD. All mutations made at S209 as well as V205L and V215A caused negative shifts in the $V_{1/2}$ of activation, whereas every other single-point mutation caused a positive shift ranging from 12 to 55 mV (Fig. 5). The effects on deactivation followed this same grouping pattern: single mutations that shifted the $V_{1/2}$ of activation to more negative potentials, now with the addition of I204A and excepting V205L, slowed deactivation with respect to WT. All of the other mutations sped deactivation at −50 mV (Fig. 5 and Table III). Similar results have been reported for the Q357R mutation in the S6 region (Boulet et al., 2006), R294H in S4, and R555C in the C terminus (Chouabe et al., 2000), but the effect of S3 mutations on the kinetics of I_{Ks} channels reported here is much more severe.

Summation of I_{Ks} at high heart rates

Ordinarily, the activation kinetics of WT I_{Ks} channels are quite slow relative to the duration of a single AP, and the deactivation kinetics allow accumulation of I_{Ks} channels in the open state during repetitive activity. This provides a "repolarizing reserve" to allow abbreviation of the cardiac AP and therefore systole, at high heart rates (Jost et al., 2005). I_{Ks} current amplitude also increases during sympathetic stimulation (Stengl et al., 2006), and block of I_{Ks} at this time lengthens the ventricular AP and prolongs the QT interval (Jost et al., 2005), suggesting that I_{Ks} is critically important for the shortening of the QT interval during sympathetic drive and tachycardia.

Ionic currents during a cardiac AP voltage clamp at 2 Hz showed that changes in mutant channel kinetics can eliminate outward I_{Ks} currents through D202N channels (Fig. 7). Although the current amplitude increased in WT channels stimulated with an AP waveform at 2 Hz, it was at 4 Hz that the ionic currents increased dramatically, and more importantly, the I_{Ks} current was present throughout the AP due to the summation effect. This increase was not observed in D202N channels and provides evidence that the D202N and the other mutations that shift the opening equilibrium positive relative to WT channels (Fig. 7) must reduce the contribution of I_{Ks} during the cardiac AP, an effect that is likely to be more pronounced at high heart rates and during stress. On the other hand, the kinetic gain-of-function mutant, S209F, causes a large increase in I_{Ks} even at 2 Hz (Fig. 8), and so were it a more stable protein, it would presumably lead to short QT syndrome or perhaps atrial fibrillation, as was recently reported in carriers of an S209P mutation (Das et al., 2009).

S3 LQT mutations in the context of the KCNQ1 structural model

There is strong evidence that the S2 and S3 transmembrane regions of Kv channels play an important role in modulating channel gating (Papazian et al., 1995; Planells-Cases et al., 1995). These domains contain acidic residues in highly conserved positions, which interact specifically with basic residues in the S4 domain to regulate channel folding and gating (Tiwari-Woodruff et al., 2000). Although the role of noncharged hydrophobic residues in the S3 domain is not fully understood, structurally there are several differences between KCNQ1 and Kv1.2 and *Shaker* channels. In addition to having fewer charges in S4, it lacks the proline in S3 that divides the helix into 3a and 3b, and it has a shorter S3–S4 linker with no negative charges (Kv1.2 and *Shaker* have four and five, respectively). Although no crystal structure exists for KCNQ1, models for its open and closed states have been developed based on Kv1.2 (Smith et al., 2007), which provides some basis for interpreting our experimental data (Figs. 1 and 9–11). In general,

Downloaded from http://rupress.org/jgp/article-pdf/135/5/433/1788272/jgp_200910351.pdf by guest on 09 February 2026

mutations at V205, I204, and V215 appear to track most closely with changes in size; therefore, it is expected that the mutations will lead to changes in packing between the helices, sometimes favoring the closed state without affecting the open state (I204A), or additionally destabilizing (I204M) the open state.

Mutations at D202

A few studies have looked at the importance of charge at equivalent positions to D202, in *Shaker*, Kv1.2 (Jogini and Roux, 2007), and KCa3.1 (Gao et al., 2008). In *Shaker*, the conserved aspartate (D316 in *Shaker*) is thought to be part of a network of long-range electrostatic interactions involving positive charges in S4 as well as additional negatively charged glutamates in S2 (Papazian et al., 1995). Thus, the negative charge at position 202 in KCNQ1 is expected to be important initially during the folding of the channel protein and then subsequently in the stabilization of the open and/or closed states. Mutation of the corresponding acidic residue in KCa3.1 to alanine results in rapid proteasomal degradation of the channel protein (Gao et al., 2008), and a D501A hERG mutant was also shown to express very poorly (Piper et al., 2008). It is therefore consistent that charge reversal, in the form of the D202H or D202K, results in channels that do not express as well and show accelerated deactivation (Table III and Figs. 3 A and 4). It is less obvious why the D202E charge-conserving mutation would result in such an extreme shift in the $V_{1/2}$ of activation and accelerated deactivation, until one considers that in the closed-channel state it appears that the side chains for D202, R195 (S2–S3 linker), and Y171 (S2) all interact in what is likely an intricate salt bridge/hydrogen-bonding arrangement (Fig. 9). In the open state, the D202–Y171 interaction appears to persist, but R195 is no longer interacting with the other two (Fig. 9, C and D), and instead R174 at the base of S2 is now involved. The kinetic changes, coupled with a normal slope factor, favor a hypothesis in which this three-way closed-state interaction is further optimized when Asp is replaced with Glu. The strengthened interaction has stabilized the closed state of these

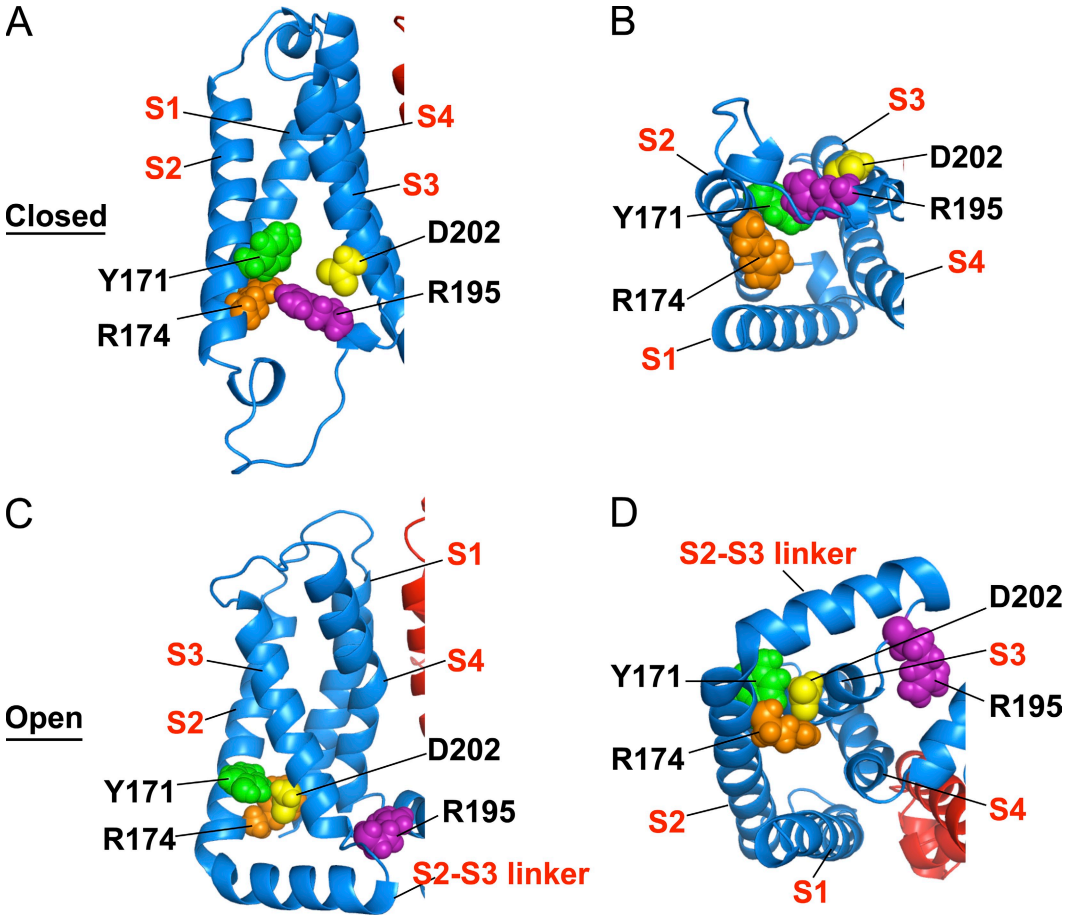

Figure 9. Molecular interactions at the cytoplasmic end of S2 and S3 are important for efficient gating of KCNQ1. D202/Y171 salt bridge/hydrogen bond with R195 in the closed state (A and B), but not in the open state (C and D). Instead, these residues now interact with R174 in the open state (C and D), an interaction not seen in the closed state (A and B). Key residues in this network of interactions are in space fill. Yellow, D202; green, Y171; magenta, R195; orange, R174. In B and D, the view is looking at the single voltage sensor domain from below.

Downloaded from http://rupress.org/jgp/article-pdf/135/5/433/1788272/jgp_200910351.pdf by guest on 09 February 2026

mutant channels, making them harder to drive into the open state.

The other naturally occurring mutant at this position in S3 is a neutralization of the charge, D202N. This mutation has the effect of accelerating both activation and deactivation kinetics (Table III), indicating that both the open and the closed state may have been affected by the loss of charge and changes in hydrogen-bonding patterns. In addition, both activation and deactivation curves have relatively little apparent voltage dependence, supporting the notion that successive electrostatic interactions may normally be formed and broken as the channel opens and closes. Indeed, in addition to direct interactions between R195/Y171 in the closed state and R174/Y171 in the open state proposed above, D202 may also be involved in other longer-range interactions. For Kv1.2 and *Shaker* channels, the equivalent residues, D259 and D316, respectively, are thought to form long-range electrostatic interactions with arginines of S4, along with a glutamate in S2 in the closed state and with K307 (Kv1.2) or K374 (*Shaker*) in the open state (Börjesson and Elinder, 2008). Preventing formation of these salt bridges might be expected to affect the stability of both states to varying degrees. In *Shaker*, D316N is able to rescue the nonfunctional K374Q mutant and results in a hyperpolarizing shift in the g-V curve, suggesting that this salt bridge is important for stabilizing the closed state (Papazian et al., 1995).

Mutations at V205

Additional mutations made at V205 (Fig. 10) proved interesting in that some resulted in channels with depolarizing shifts in $V_{1/2}$'s of activation (V205M and V205A; Figs. 3 C and 5) and one hyperpolarizing shift (V205L). Energy minimization after making the equivalent mutations at position 205 in the model resulted in subtle changes to the position in the backbones of the TMDs (Fig. 10), with V205A allowing S2 and S3 to shift apart slightly, whereas in V205L they appeared to be somewhat closer in the closed state. A comparison of the residues in contact with R195 and D202, sites involved in

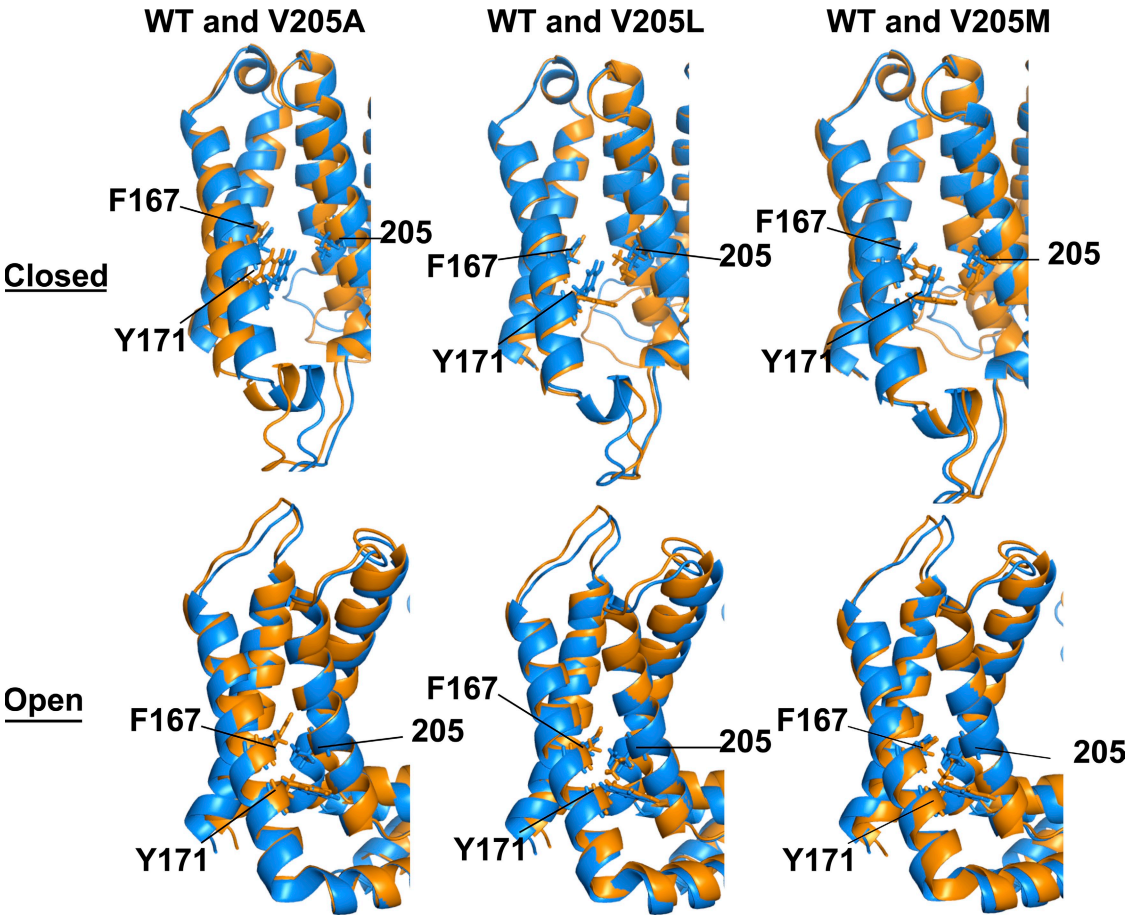

Figure 10. Model predictions for the effect of mutations at V205 on voltage sensor transmembrane domain backbone structure. Mutations were made in the KCNQ1 homology models, and then subjected to side chain repacking and gradient energy minimization, including the WT channel. Resulting closed- (top row) and open-state (bottom row) mutant structures were then overlain on the WT channel backbone structure. WT channel is blue, and mutant channels are orange. The residue at position 205 is shown in bonds-only mode, as are F167 and Y171 in S2.

Downloaded from http://rupress.org/jgp/article-pdf/135/5/433/1788272/jgp_200910351.pdf by guest on 09 February 2026

the salt bridge/hydrogen bond that stabilizes the closed state (Table S2), showed a pattern in which close interactions between the cytosolic ends of S2 and S3 as well as the S2–S3 linker, centered around the highly conserved, positively charged residue in this linker (R195 in KCNQ1), are associated with more hyperpolarized $V_{1/2}$'s of activation (V205L and V205). Loss of this network of interactions in V205A leads to a 50-mV depolarizing shift in the $V_{1/2}$ of activation for the mutant channel. This does not explain why V205M, which is not expected to disrupt this network, also has a right-shifted g-V curve. However, energy-minimized structures of this mutant show an additional interaction in the closed state not seen in the others. V205M is predicted to also interact with F167 in the middle of S2 (Table S2), an interaction that may serve to further stabilize the closed state and prevent S3 from moving as efficiently. In addition, this phenylalanine in S2, which is 99% conserved in Kv channels (Lee et al., 2009), in our model makes what are obviously functionally important contacts with S4 and S1 residues in the closed and open states. These F167 interactions with S1 (V129, I132, and V133) and S4 (Q234 and M238) are lost in the closed state of V205M, but the open-state interactions are maintained (V129, I132, V133, and H240). In the WT channel, V205 is predicted to interact with Y171 in S2 (Fig. S3), but this interaction is lost in V205L, further supporting the concept that interhelical interactions at this position slow channel activation.

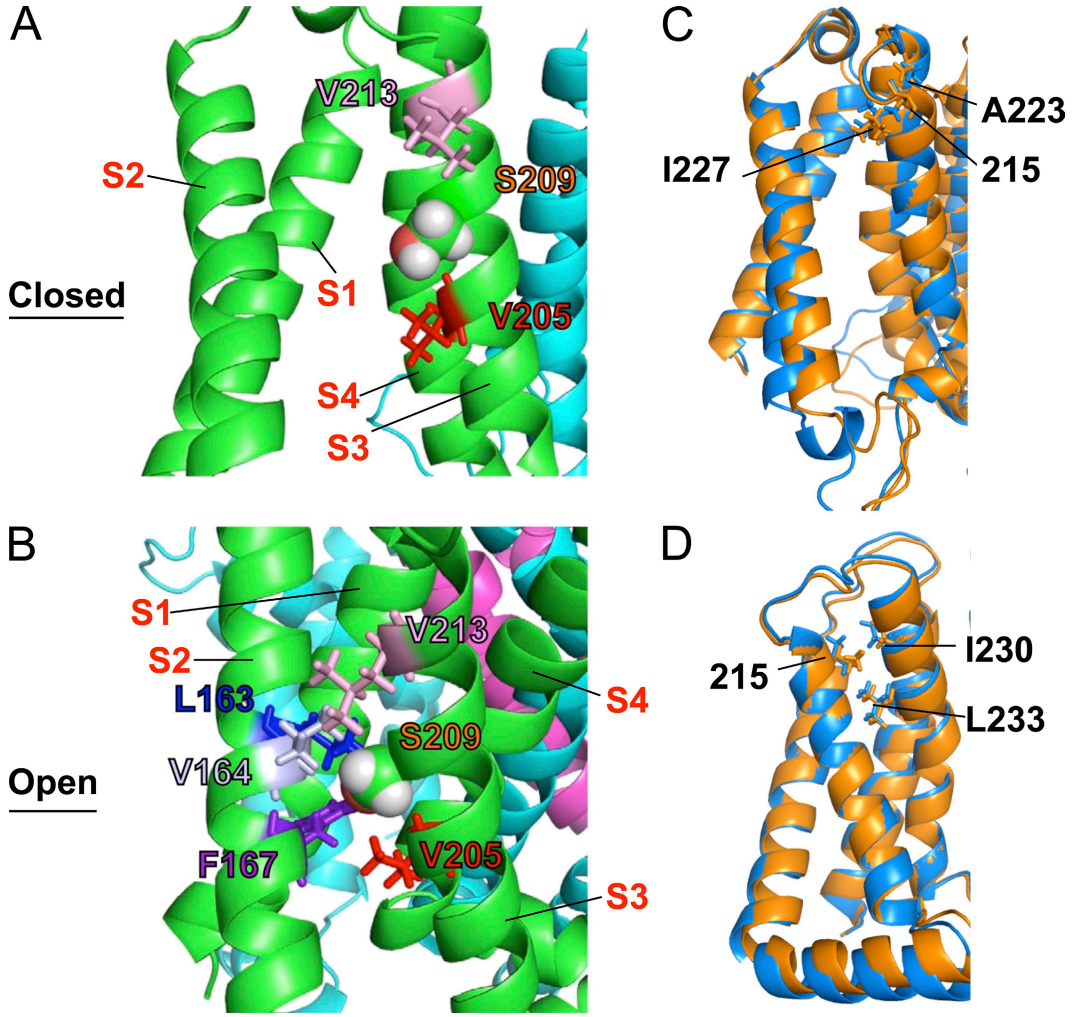

Figure 11. Molecular interactions for S209 and V215 from the KCNQ1 homology model. Polar S209 moves to a hydrophobic pocket in the open state. (A) Close-up view of the residues within van der Waals contact of S209 in the *KCNQ1* closed- and (B) open-state models. S209 from the green subunit is in space fill. Residues determined to have side chains in Van der Waals contact (see Materials and methods) with the side chain of S209 are labeled and have side chains shown in bonds-only mode. (C and D) The KCNQ1 models predict that V215M can be accommodated in the closed state but perturbs the open state. The V215M mutation was made in the KCNQ1 homology models, and the WT and mutant channel were then subjected to side chain repacking and gradient energy minimization. The WT channel is in blue, and V215M is in orange. The amino acids at 215 as well as A223, I227, I230, and L233 are shown in bonds-only mode.

Downloaded from http://rupress.org/jgp/article-pdf/135/5/433/1788272/jgp_200910351.pdf by guest on 09 February 2026

Experiments involving neutralization of the Shaker S3 residue D316 to N316 (D202 in KCNQ1) resulted in a decrease of approximately two proton charges per channel (Seoh et al., 1996), indicating that neutralization either caused repositioning of S4 or that S3 is also contributing to gating. If S3 also moves during gating and S1–S2 are indeed the largely stationary component of the voltage sensor domain involved in bracing the moveable component (Lee et al., 2009), disrupting certain "bracing" interactions between S2 and S3 might affect coupling between depolarization and gating, as seen for the V205A mutant.

Mutations at S209

In the open state, S209 is deeply buried in the hydrophobic core (Fig. 11 B). This is the region, including a turn of the helix down at V205, where S3 makes its closest approach to S2 in the open state. It is not uncommon for a serine or alanine to be at such a position within TMD helix interfaces (Adamian and Liang, 2001). In the closed state, S209 is partially exposed to the protein surface, where it may be able to hydrogen bond with water. All the mutations at this position lead to strong bias toward channel opening at all potentials (Fig. 5 and Table III). All the mutations were to hydrophobic residues, but they varied greatly in size from similar to Ser (Ala), to much larger residues. Ser209Ala led to the smallest shift in $V_{1/2}$ and kinetics, whereas the introduction of bulkier and more hydrophobic side chains led to even greater negative shifts in the $V_{1/2}$ of activation. We suggest that the impact of the Ser209-to-apolar substitutions on the energy of the closed state is likely to destabilize the closed state as a result of loss of hydrogen bonding in this state. At the same time, Ser-to-apolar substitutions are likely to stabilize the open state by relieving energetic frustration that stems from burying a hydroxyl side chain in a hydrophobic environment without a hydrogen-bonding partner. By both destabilizing the closed state and stabilizing the open state, Ser-to-hydrophobic substitutions result in gain-of-function channel behavior.

Mutations at V215

The region of the channel including V215 in our models is quite interesting in that in the closed state, this region is somewhat unstructured, but when the channel opens it becomes part of the S3 helix (Fig. 11, C and D). Putting a proline (a helix breaker) at this position resulted in a 40-mV positive shift in the $V_{1/2}$ of activation but faster activation and deactivation in the physiological range (similar to V215M shown in Figs. 3 B, 4 B, and 5, and Table III), indicating that the proline has at least affected the stability of the open state. The V215M mutation results in a 20-mV positive shift in activation, and in the model it shows little change in the closed-state structure (Fig. 11 C). Although the closed state appears to accommodate the bulkier side chain of methionine, the open state is more perturbed, with methionine making more contacts with the S3–S4 linker and S4, creating subtle repositioning of S3 with respect to S2 and S4 (Fig. 11 D) and destabilizing the open state. On the other hand, the V215A mutation shifts the $V_{1/2}$ in the opposite direction slightly, suggesting that the less constrained S4 is by interactions with the carboxyl end of S3, the more stable the open state. Consistent with this, deactivation rates for V215A approach three times that of the WT channel (Fig. 5).

We thank Dr. Saman Rezazadeh for help with preliminary data and studies. We also thank Ms. Ka Kee Chiu and Ms. KyungHee Park for preparation of cells.

This work was supported by the Heart and Stroke Foundation of British Columbia and Yukon (HSFBC&Y) and Canadian Institutes of Health Research grants to D. Fedida. D. Fedida is supported by the HSFBC&Y. C. Kang and C. Sanders were supported by National Institutes of Health grant RO1 DC007416. G.F. Tibbits is a Canada Research Chair.

Christopher Miller served as editor.

Submitted: 27 October 2009
Accepted: 31 March 2010

REFERENCES

Ackerman, M.J., D.J. Tester, G.S. Jones, M.L. Will, C.R. Burrow, and M.E. Curran. 2003. Ethnic differences in cardiac potassium channel variants: implications for genetic susceptibility to sudden cardiac death and genetic testing for congenital long QT syndrome. *Mayo Clin. Proc.* 78:1479–1487. doi:10.4065/78.12.1479

Adamian, L., and J. Liang. 2001. Helix-helix packing and interfacial pairwise interactions of residues in membrane proteins. *J. Mol. Biol.* 311:891–907. doi:10.1006/jmbi.2001.4908

Arbour, L., S. Rezazadeh, J. Eldstrom, G. Weget-Simms, R. Rupps, Z. Dyer, G. Tibbits, E. Accili, B. Casey, A. Kmetic, et al. 2008. A KCNQ1 V205M missense mutation causes a high rate of long QT syndrome in a First Nations community of northern British Columbia: a community-based approach to understanding the impact. *Genet. Med.* 10:545–550. doi:10.1097/GIM.0b013e31817c6b19

Arking, D.E., A. Pfeufer, W. Post, W.H. Kao, C. Newton-Cheh, M. Ikeda, K. West, C. Kashuk, M. Akyol, S. Perz, et al. 2006. A common genetic variant in the NOS1 regulator NOS1AP modulates cardiac repolarization. *Nat. Genet.* 38:644–651. doi:10.1038/ng1790

Börjesson, S.I., and F. Elinder. 2008. Structure, function, and modification of the voltage sensor in voltage-gated ion channels. *Cell Biochem. Biophys.* 52:149–174. doi:10.1007/s12013-008-9032-5

Boulet, I.R., A.L. Raes, N. Ottschytsch, and D.J. Snyders. 2006. Functional effects of a KCNQ1 mutation associated with the long QT syndrome. *Cardiovasc. Res.* 70:466–474. doi:10.1016/j.cardiores.2006.02.006

Chouabe, C., N. Neyroud, P. Richard, I. Denjoy, B. Hainque, G. Romey, M.D. Drici, P. Guicheney, and J. Barhanin. 2000. Novel mutations in KvLQT1 that affect Iks activation through interactions with Isk. *Cardiovasc. Res.* 45:971–980. doi:10.1016/S0008-6363(99)00411-3

Dahimène, S., S. Alcoléa, P. Naud, P. Jourdon, D. Escande, R. Brasseur, A. Thomas, I. Baró, and J. Mérot. 2006. The N-terminal juxtamembranous domain of KCNQ1 is critical for channel surface expression: implications in the Romano-Ward

Downloaded from http://rupress.org/jgp/article-pdf/135/5/433/1788272/jgp_200910351.pdf by guest on 09 February 2026

LQT1 syndrome. *Circ. Res.* 99:1076–1083. doi:10.1161/01.RES.0000250262.12219.95

Das, R., and D. Baker. 2008. Macromolecular modeling with rosetta. *Annu. Rev. Biochem.* 77:363–382. doi:10.1146/annurev.biochem.77.062906.171838

Das, S., S. Makino, Y.F. Melman, M.A. Shea, S.B. Goyal, A. Rosenzweig, C.A. Macrae, and P.T. Ellinor. 2009. Mutation in the S3 segment of KCNQ1 results in familial lone atrial fibrillation. *Heart Rhythm.* 6:1146–1153. doi:10.1016/j.hrthm.2009.04.015

DeLano, W.L. 2002. PyMOL Molecular Viewer. http://www.pymol.org (accessed April 1, 2010).

Ellgaard, L., and A. Helenius. 2003. Quality control in the endoplasmic reticulum. *Nat. Rev. Mol. Cell Biol.* 4:181–191. doi:10.1038/nrm1052

Gao, Y., C.K. Chotoo, C.M. Balut, F. Sun, M.A. Bailey, and D.C. Devor. 2008. Role of S3 and S4 transmembrane domain charged amino acids in channel biogenesis and gating of KCa2.3 and KCa3.1. *J. Biol. Chem.* 283:9049–9059. doi:10.1074/jbc.M708022200

Jogini, V., and B. Roux. 2007. Dynamics of the Kv1.2 voltage-gated K+ channel in a membrane environment. *Biophys. J.* 93:3070–3082. doi:10.1529/biophysj.107.112540

Jost, N., L. Virág, M. Bitay, J. Takács, C. Lengyel, P. Biliczki, Z. Nagy, G. Bogáts, D.A. Lathrop, J.G. Papp, and A. Varró. 2005. Restricting excessive cardiac action potential and QT prolongation: a vital role for IKs in human ventricular muscle. *Circulation.* 112:1392–1399. doi:10.1161/CIRCULATIONAHA.105.550111

Kang, C., C. Tian, F.D. Sönnichsen, J.A. Smith, J. Meiler, A.L. George Jr., C.G. Vanoye, H.J. Kim, and C.R. Sanders. 2008. Structure of KCNE1 and implications for how it modulates the KCNQ1 potassium channel. *Biochemistry.* 47:7999–8006. doi:10.1021/bi800875q

Kuhlman, B., and D. Baker. 2000. Native protein sequences are close to optimal for their structures. *Proc. Natl. Acad. Sci. USA.* 97:10383–10388. doi:10.1073/pnas.97.19.10383

Lee, S.Y., A. Banerjee, and R. MacKinnon. 2009. Two separate interfaces between the voltage sensor and pore are required for the function of voltage-dependent K(+) channels. *PLoS Biol.* 7:e47. doi:10.1371/journal.pbio.1000047

Lehnart, S.E., M.J. Ackerman, D.W. Benson Jr., R. Brugada, C.E. Clancy, J.K. Donahue, A.L. George Jr., A.O. Grant, S.C. Groft, C.T. January, et al. 2007. Inherited arrhythmias: a National Heart, Lung, and Blood Institute and Office of Rare Diseases workshop consensus report about the diagnosis, phenotyping, molecular mechanisms, and therapeutic approaches for primary cardiomyopathies of gene mutations affecting ion channel function. *Circulation.* 116:2325–2345. doi:10.1161/CIRCULATIONAHA.107.711689

Long, S.B., E.B. Campbell, and R. Mackinnon. 2005. Voltage sensor of Kv1.2: structural basis of electromechanical coupling. *Science.* 309:903–908. doi:10.1126/science.1116270

Manganas, L.N., and J.S. Trimmer. 2000. Subunit composition determines Kv1 potassium channel surface expression. *J. Biol. Chem.* 275:29685–29693. doi:10.1074/jbc.M005010200

Napolitano, C., S.G. Priori, P.J. Schwartz, R. Bloise, E. Ronchetti, J. Nastoli, G. Bottelli, M. Cerrone, and S. Leonardi. 2005. Genetic testing in the long QT syndrome: development and validation of an efficient approach to genotyping in clinical practice. *JAMA.* 294:2975–2980. doi:10.1001/jama.294.23.2975

Newton-Cheh, C., M. Eijgelsheim, K.M. Rice, P.I. de Bakker, X. Yin, K. Estrada, J.C. Bis, K. Marciante, F. Rivadeneira, P.A. Noseworthy, et al. 2009. Common variants at ten loci influence QT interval duration in the QTGEN Study. *Nat. Genet.* 41:399–406. doi:10.1038/ng.364

Nishio, H., M. Kuwahara, H. Tsubone, Y. Koda, T. Sato, S. Fukunishi, A. Tamura, and K. Suzuki. 2009. Identification of an ethnic-specific variant (V207M) of the KCNQ1 cardiac potassium channel gene in sudden unexplained death and implications from a knock-in mouse model. *Int. J. Legal Med.* 123:253–257. doi:10.1007/s00414-009-0321-3

Papazian, D.M., X.M. Shao, S.-A. Seoh, A.F. Mock, Y. Huang, and D.H. Wainstock. 1995. Electrostatic interactions of S4 voltage sensor in Shaker K^+ channel. *Neuron.* 14:1293–1301. doi:10.1016/0896-6273(95)90276-7

Piper, D.R., J. Rupp, F.B. Sachse, M.C. Sanguinetti, and M. Tristani-Firouzi. 2008. Cooperative interactions between R531 and acidic residues in the voltage sensing module of hERG1 channels. *Cell. Physiol. Biochem.* 21:37–46. doi:10.1159/000113745

Planells-Cases, R., A.V. Ferrer-Montiel, C.D. Patten, and M. Montal. 1995. Mutation of conserved negatively charged residues in the S2 and S3 transmembrane segments of a mammalian K^+ channel selectively modulates channel gating. *Proc. Natl. Acad. Sci. USA.* 92:9422–9426. doi:10.1073/pnas.92.20.9422

Rossenbacker, T., and S.G. Priori. 2007. Clinical diagnosis of long QT syndrome: back to the caliper. *Eur. Heart J.* 28:527–528. doi:10.1093/eurheartj/ehl552

Sanguinetti, M.C., M.E. Curran, A. Zou, J. Shen, P.S. Spector, D.L. Atkinson, and M.T. Keating. 1996. Coassembly of $K_{(V)}$LQT1 and minK (IsK) proteins to form cardiac $I_{(Ks)}$ potassium channel. *Nature.* 384:80–83. doi:10.1038/384080a0

Seoh, S.A., D. Sigg, D.M. Papazian, and F. Bezanilla. 1996. Voltage-sensing residues in the S2 and S4 segments of the *Shaker* K^+ channel. *Neuron.* 16:1159–1167. doi:10.1016/S0896-6273(00)80142-7

Shalaby, F.Y., P.C. Levesque, W.P. Yang, W.A. Little, M.L. Conder, T. Jenkins-West, and M.A. Blanar. 1997. Dominant-negative KvLQT1 mutations underlie the LQT1 form of long QT syndrome. *Circulation.* 96:1733–1736.

Smith, J.A., C.G. Vanoye, A.L. George Jr., J. Meiler, and C.R. Sanders. 2007. Structural models for the KCNQ1 voltage-gated potassium channel. *Biochemistry.* 46:14141–14152. doi:10.1021/bi701597s

Stengl, M., C. Ramakers, D.W. Donker, A. Nabar, A.V. Rybin, R.L. Spätjens, T. van der Nagel, W.K. Wodzig, K.R. Sipido, G. Antoons, et al. 2006. Temporal patterns of electrical remodeling in canine ventricular hypertrophy: focus on IKs downregulation and blunted beta-adrenergic activation. *Cardiovasc. Res.* 72:90–100. doi:10.1016/j.cardiores.2006.07.015

Tester, D.J., and M.J. Ackerman. 2009. Cardiomyopathic and channelopathic causes of sudden unexplained death in infants and children. *Annu. Rev. Med.* 60:69–84. doi:10.1146/annurev.med.60.052907.103838

Tester, D.J., M.L. Will, C.M. Haglund, and M.J. Ackerman. 2005. Compendium of cardiac channel mutations in 541 consecutive unrelated patients referred for long QT syndrome genetic testing. *Heart Rhythm.* 2:507–517. doi:10.1016/j.hrthm.2005.01.020

Tiwari-Woodruff, S.K., M.A. Lin, C.T. Schulteis, and D.M. Papazian. 2000. Voltage-dependent structural interactions in the *Shaker* K^+ channel. *J. Gen. Physiol.* 115:123–138. doi:10.1085/jgp.115.2.123

Yamaguchi, M., M. Shimizu, H. Ino, H. Terai, K. Hayashi, H. Mabuchi, N. Hoshi, and H. Higashida. 2003. Clinical and electrophysiological characterization of a novel mutation (F193L) in the KCNQ1 gene associated with long QT syndrome. *Clin. Sci. (Lond.).* 104:377–382. doi:10.1042/CS20020152

Yarov-Yarovoy, V., D. Baker, and W.A. Catterall. 2006. Voltage sensor conformations in the open and closed states in ROSETTA structural models of K(+) channels. *Proc. Natl. Acad. Sci. USA.* 103:7292–7297. doi:10.1073/pnas.0602350103

Downloaded from http://rupress.org/jgp/article-pdf/135/5/433/1788272/jgp_200910351.pdf by guest on 09 February 2026